CRYSTAL Research&Technology
www.crt-journal.org

Stimulated Raman Scattering (SRS) in α-AlOOH (Diaspore)

Ladislav Bohatý, Oliver Lux, Hans-Joachim Eichler, Hanjo Rhee, Alexander A. Kaminskii†, and Petra Becker**

In single crystals of orthorhombic α-AlOOH, known also as mineral diaspore, $\chi^{(3)}$-nonlinear lasing by stimulated Raman scattering (SRS) and Raman-induced four-wave mixing (RFWM) is investigated. Picosecond pumping at 1.064 µm wavelength produces a broadband Stokes and anti-Stokes frequency comb with up to 25 SRS- and RFWM-generated emission lines. All observed Stokes and anti-Stokes lasing components in the visible and near-IR are identified and attributed to a single SRS-promoting vibration mode with $\omega_{SRS} \approx 445$ cm^{-1}. The first Stokes steady-state Raman gain coefficient in the visible spectral range is estimated to a value not less than 0.36 cm GW^{-1}.

1. Introduction

Nonlinear $\chi^{(3)}$-lasing processes by stimulated Raman scattering (SRS) and Raman-induced four-wave mixing (RFWM) have been studied in a large variety of crystals in the last two decades (for an overview see, e.g., ref. [1]). The generated SRS emission lines cover the broad region from ≈0.2 to ≈2 µm and result from SRS-active vibration modes with energies that range between ≈50 and ≈3400 cm^{-1}. The Raman shifts of these SRS-active Raman modes, however, are not distributed equally within the so far realized energy range and there are only few materials, e.g., α-quartz ($\omega_{SRS} \approx 465$ cm^{-1} [2]) and α-Al_2O_3 ($\omega_{SRS} \approx 419$ cm^{-1} [3,4]), that possess SRS-promoting vibration modes of around 450 cm^{-1}. Here, α-AlOOH, which shows a strong, sharp, and isolated vibration mode at 446 cm^{-1} in its spontaneous Raman spectra,[5] appears to be a promising further material which could complement the set of SRS materials in this region. In addition, among the variety of studied SRS crystals, materials which possess large Raman shifts of around 3000 cm^{-1} are of interest, since they are able to generate the first Stokes component in the eye-safe region starting from 1 µm pumping wavelengths. Here, the question arises, whether O—H stretching vibrations of intermediate hydrogen bonds, that have typical energy values of 2800–3100 cm^{-1},[6] can act as SRS-active vibration modes in crystals. To the best of our knowledge neither for organic, for semi-organic nor for inorganic crystals, that have been studied by SRS so far, SRS-promoting modes of O—H stretching vibrations has been detected.

As has been shown in detailed investigations based on experimental data (IR and spontaneous Raman spectroscopy, inelastic X-ray scattering) and theoretical calculations[6–9] α-AlOOH is a suitable model system to study O—H groups in intermediate hydrogen bonds due to its rather simple chemistry and crystal structure.[6] A possible limitation of the applicability of this model system to the study of potential SRS-activity of O—H vibration modes is given by the broadness of O—H stretching vibrations in α-AlOOH found in spontaneous Raman spectra by ref. [5], since the Raman gain coefficient for generation of the first Stokes components via SRS is proportional to the inverse of the linewidth of the SRS-promoting vibration mode in the spontaneous Raman spectrum.[10] However, this precept is not exclusionary, as has been shown, e.g., in ref. [11], where also weak and broad vibration modes of the spontaneous Raman spectrum gave rise to stimulated Raman scattering. In this work, we present an experimental study of stimulated Raman scattering in single crystals of α-AlOOH, also known as mineral diaspore.

2. Crystals of α-AlOOH

Diaspore (α-AlOOH) had been subject of structural investigations by X-ray diffraction already since the early 1930s.[12–17] Correct localization of hydrogen atoms in the crystal structure using neutron diffraction was first achieved by ref. [18]. In the

L. Bohatý, P. Becker
Section Crystallography
Institute of Geology and Mineralogy, University of Cologne
50939 Köln, Germany
E-mail: ladislav.bohaty@uni-koeln.de; petra.becker@uni-koeln.de
O. Lux, H.-J. Eichler, H. Rhee
Institute of Optics and Atomic Physics
Technical University of Berlin
10623 Berlin, Germany
O. Lux
Deutsches Zentrum für Luft- und Raumfahrt
Institut für Physik der Atmosphäre
82234 Oberpfaffenhofen, Germany
A. A.
Institute of Crystallography, Federal Scientific Center "Crystallography and Photonics"
Russian Academy of Sciences
Moscow 119333, Russia

The ORCID identification number(s) for the author(s) of this article can be found under https://doi.org/10.1002/crat.202100055

†A. A. Kaminskii passed away during the present work.

DOI: 10.1002/crat.202100055

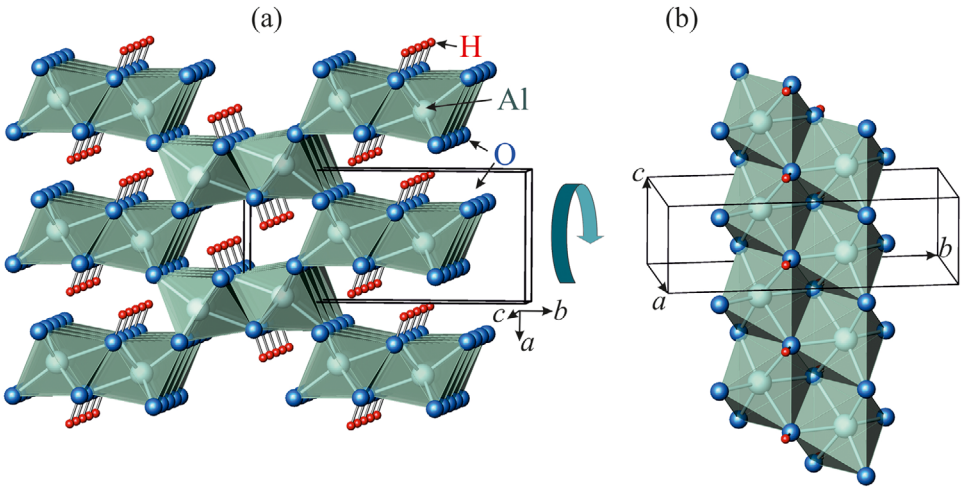

Figure 1. Graphical representation of the crystal structure of α-AlOOH, structure data are taken from ref. [20]. Al is given by gray spheres; O ligands are given by blue spheres and H is given by small red spheres. Distorted octahedral coordination polyhedra $[AlO_3(OH)_3]$ are indicated. a) View approximately along the *c*-axis showing the connection scheme of double chains, running along the *c*-axis, of $[AlO_3(OH)_3]$ octahedra. b) View approximately along the *a*-axis, visualizing the linkage of $[AlO_3(OH)_3]$ to double chains by sharing common edges.

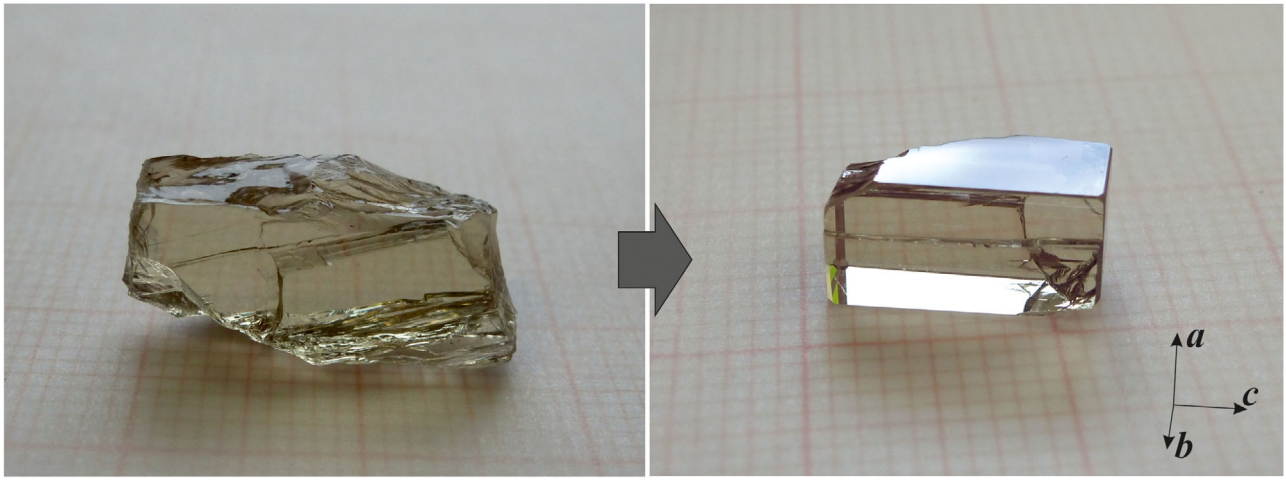

Figure 2. Left: Gem-quality natural single crystal of α-AlOOH (diaspore) used for preparation of samples for the investigations in this work. (Small squares give 1×1 mm^2). Right: Sample of α-AlOOH, prepared from the crystal on the left and used for SRS and RFWM measurements. Sample faces were polished but without antireflection coating.

following, a number of structural refinements and structural investigations under nonambient conditions have been performed (for a compilation see ref. [19]). In the present work, we use structure data taken from ref. [20].

Crystals of α-AlOOH crystallize with orthorhombic space group symmetry *Pbnm* (setting *cab*), with lattice constants $a = 4.4007(6)$ Å, $b = 9.4253(13)$ Å, and $c = 2.8452(3)$ Å.[20] The main structural feature of α-AlOOH is double-chains of $[AlO_3(OH)_3]$ octahedra, where each aluminum coordination octahedron shares common edges with four adjacent octahedra (see **Figure 1**b). The double chains that run along the *c*-axis are linked via common corners (i.e., oxygen atoms) to a 3D network, as it is illustrated in Figure 1a.

Because of its relevance for both, geo-sciences and technical applications, the system Al_2O_3–H_2O has been studied intensively already many years ago, see, e.g., refs. [21–25]. Therefore, the range of thermodynamic stability as well as the possibility of crystallization of α-AlOOH under hydrothermal conditions is well known. While the preparation of small (sub-mm size) crystals has been performed, see, e.g., ref. [26], the growth of large ($\geq$1 cm^3) single crystals of α-AlOOH, which would require considerable expenditure, is not reported in literature so far. Fortunately, large crystals of α-AlOOH (mineral diaspore) of optical (gem-stone) quality can be found in some localities in nature. For the present work we used a single crystal of gem-quality diaspore (see **Figure 2**, left) from Turkey, Muğla Province, which is described as locality in ref. [27].

Gem-quality crystals from this locality typically contain up to $\approx$0.1% of Fe^{3+},[28,29] which substitutes Al^{3+} in the crystal structure. Low iron content in α-AlOOH and similarly in α-Al_2O_3 (corundum) is known to cause weak absorption bands at $\approx$384 nm and $\approx$398 nm in α-AlOOH and $\approx$377 nm and $\approx$388 nm

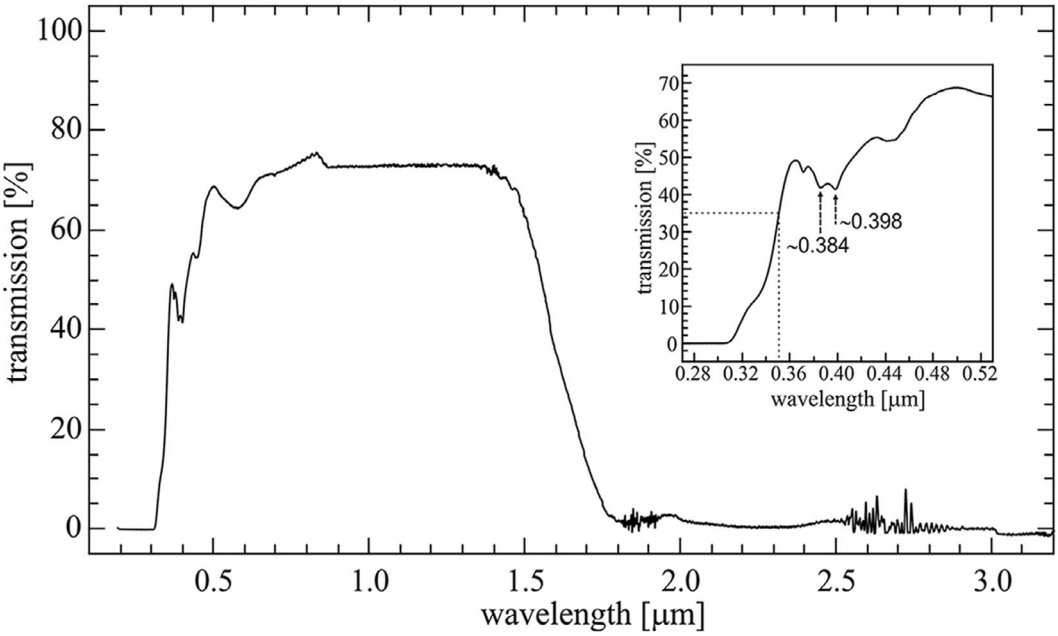

Figure 3. Transmission spectrum of the used natural single crystal of α-AlOOH in orientation (001) with 1.37 mm thickness. The inset gives a magnification of the short wavelength region, with indicated UV transmission limit at 50% of maximum transmission (dashed lines). The arrows mark two absorption peaks that, according to ref. [28], can be attributed to Fe^{3+} in diaspore.

in α-Al_2O_3, respectively.[28,30,31] Nonpolarized optical transmission data of our crystal were collected using a polished plate of orientation (001) of 1.37 mm thickness and a spectrophotometer Perkin Elmer Lambda 950. The transmission spectrum is given in **Figure 3**. Optical transmission of α-AlOOH ranges from ≈0.35 μm (50% of maximum transmission level) to ≈1.5 μm. The transmission data show weak absorption bands in the near UV similar to those reported in ref. [28] (see inset of Figure 3), which signalize a small content of Fe^{3+} in our used crystal. Due to its orthorhombic symmetry α-AlOOH is optically biaxial and, as calculated from refractive indices, possesses positive character of birefringence with an angle $2V_\gamma$ between the optic axes ranging between 83.5° ($\lambda = 0.4358$ μm) and 82.8° ($\lambda = 0.6438$ μm). Refractive index data of diaspore are given in literature for wavelengths in the visible range (λ = 0.4358–0.6438 μm)[29,32] and are compiled in **Table 1**, together with selected further physical properties of α-AlOOH crystals.

For the measurement of SRS and RFWM spectra a rectangular parallel-epipedal sample was prepared with face normals along the orthorhombic axes *a*, *b* , and *c* and with dimensions 5.74 × 5.79 × 11.09 mm^3 (see Figure 2, right). All sample faces were polished but without antireflection coating.

3. Stimulated Raman Scattering

3.1. Experimental Setup

The spectroscopic investigation of $\chi^{(3)}$-nonlinear processes in α-AlOOH was performed using a mode-locked Nd^{3+}:$Y_3Al_5O_{12}$ master oscillator power amplifier system in combination with a spectrometric setup, as described in previous publications (see, e.g., refs. [35, 36]). The pump laser system operated at 1 Hz repetition rate, providing single pulses at $\lambda_{f1} = 1.06415$ μm wavelength with pulse energy of up to 40 mJ and pulse duration of about 80 ps. The pump beam was guided to the registration part of the experimental setup which is shown in **Figure 4**a. Here, continuous attenuation of the pump was realized with the combination of a revolving half-wave-plate ($\lambda_{f1}/2$) and a Glan-laser polarizer (P), while the pump energy incident on the α-AlOOH sample was monitored by measuring a small portion of the radiation using a pyroelectric energy meter (Polytec RjP-735). The linearly polarized and collimated, nearly Gaussian beam was then focused into the α-AlOOH crystal using a planoconvex lens with a focal length of f_{L1} = 250 mm. The sample could be aligned at any angle with respect to the pump beam direction and polarization by means of a customized 3D-adjustable holder. A lens system consisting of a spherical biconvex lens (f_{L2} = 100 mm) and a planoconvex cylindrical lens (f_{L3} = 100 mm) was employed to collimate the divergent output radiation and to image it onto the variable entrance slit of a monochromator in Czerny-Turner arrangement (McPherson Model 270, 6.8 Å $pixel^{-1}$ dispersion, 150 lines mm^{-1} grating). The spectral composition of the scattered emission was finally recorded by a silicon (Si)-CCD sensor (Hamamatsu S3924-1024Q with 1024 pixels) for the UV and visible spectral region and an InGaAs sensor (Hamamatsu G9204-512D with 512 pixels) for the range between 0.9 and 1.7 μm, respectively (see Figure 4b). For the energy calibration of the recorded Stokes and anti-Stokes components the laser emission wavelengths at 0.63282 and 0.54337 μm (He-Ne laser) in the visible range, and at 1.06415 μm (Nd^{3+}:YAG), 1.3166 μm ($Ba(NO_3)_2$ Raman laser), and 1.5987 μm (Er^{3+}:$GdVO_4$) in the IR region were used.

3.2. Results

All registered Stokes and anti-Stokes sidebands in the measured spectra were identified and attributed to a single SRS-promoting

Table 1. Selected physical properties of α-AlOOH (diaspore) at room temperature.

Property	Value			
Chemical composition[28,29]	AlOOH (synthetic), gem diaspore from Turkey with traces of Fe^{3+}			
Space group[13]	*Pbmn* $-D_{2h}^{16}$ (No. 62)			
Unit cell parameters[20] [Å]	$a = 4.4007(6)$			
	$b = 9.4253(13)$			
	$c = 2.8452(3)$			
Formula units per unit cell[13]	$Z = 4$			
Fractional coordinates *x*, *y*, *z*, and site symmetry (ss)[20]	*x*	*y*	*z*	ss
	Al 0.04472(8)	−0.14450(4)	−0.25	4*c* (*m*)
	O1 0.71234(17)	0.19892(9)	−0.25	4*c* (*m*)
	O2 0.19714(18)	0.05338(9)	−0.25	4*c* (*m*)
	H 0.4095	0.0876	−0.25	4*c* (*m*)
Density[33] [g cm^{-3}]	3.388(2)			
Cleavage (see, e.g.,[25,34])	{010} perfect			
Hardness (Mohs scale; see, e.g.,[25,34])	6.5–7			
Thermal expansion at 293 K[33] [10^{-6} K^{-1}]	$\alpha_{11} = 7.5$ (5)	$\alpha_{22} = 6.5$ (5)	$\alpha_{33} = 6.0$ (5)	
Optical transparency range [µm]	≈0.35 to ≈1.50			

Refractive indices (Sellmeier coefficients)[a]		D_1	D_2	D_3	D_4	ξ^2
ξ^2 is the sum of the squares of the residuals	$n_\alpha = n_c$	2.84(3)	0.020(9)	−0.01(4)	−0.002(4)	8.2×10^{-9}
	$n_\beta = n_b$	2.78(8)	0.08(4)	−0.16(8)	−0.12(7)	6.1×10^{-9}
	$n_\gamma = n_a$	2.99(2)	0.028(6)	−0.03(2)	0.008(2)	2.1×10^{-9}
Optical nonlinearity	$\chi^{(3)}$					
Energy of SRS-promoting vibration modes at room temperature ω_{SRS} [cm^{-1}]	≈445					
FWHM linewidth $\Delta\nu_R$ for the Raman shifted line related to SRS-promoting vibration mode [cm^{-1}]	8					
Steady-state Raman gain coefficient for first Stokes generation [cm GW^{-1}] at a pump wavelength $\lambda_f = 1.06415$ µm	≥0.36					

[a] Sellmeier coefficients with respect to the modified Sellmeier equation (λ is in µm) $n^2(\lambda) = D_1 + \frac{D_2}{(\lambda^2 - D_3)} - D_4\lambda^2$, calculated using refractive index data in the visible range given in ref. [32].

phonon mode. The Raman shift ω_{SRS} of this SRS-active vibration mode was determined as the mean value resulting from all analyzed SRS and RFWM spectra of the used α-AlOOH single crystal and amounts to $\omega_{SRS} = 445(2)$ cm^{-1}. Selected $\chi^{(3)}$-nonlinear lasing spectra, recorded at room temperature with 1 µm picosecond pumping in different excitation geometries, together with the results of their spectral analysis are presented in **Figures 5–7**. The attribution of all observed Stokes and anti-Stokes components to SRS and RFWM processes are summarized in **Tables 2** and **3**.

As can be seen from Figure 5, picosecond pumping at $\lambda_{f1} = 1.06415$ µm wavelength of the AlOOH crystal, with an SRS active length of ≈11 mm in excitation geometry *c*(*a*,*a*)*c* (for the used notation see footnote a) in Table 2), gave rise to single-phonon $\chi^{(3)}$-nonlinear lasing with $\omega_{SRS} \approx 445$ cm^{-1}. As many as 17 anti-Stokes and four Stokes sidebands were recorded under these excitation conditions (see Table 2). Using excitation geometry *c*(*b*,*b*)*c* (see Figures 6 and 7) the SRS-active mode with $\omega_{SRS} \approx 445$ cm^{-1} led to the generation of an even broader frequency comb consisting of 21 anti-Stokes and six Stokes components (see Table 3). The latter was produced by cascaded $\chi^{(3)}$ interactions (most probably RFWM processes) and covers nearly one spectral octave (more than 12 000 cm^{-1}). In Tables 2 and 3, the most likely RFWM processes for each observed spectral component are given.

The spatial distribution of the broadband anti-Stokes emission generated with pumping at $\lambda_{f1} = 1.06415$ µm wavelength in excitation geometry *c*(*b*,*b*)*c* and given in Figure 7 was analyzed using a CCD photocamera (Panasonic, model Lumix DMC-TZ7). The camera recorded the radiation reflected from a screen which was inserted behind the α-AlOOH sample. As shown in **Figure 8**, the anti-Stokes components, which are predominantly originated by RFWM, are emitted along cones whose opening angles increase with the anti-Stokes order as a result of momentum conservation in the presence of normal dispersion. The corresponding

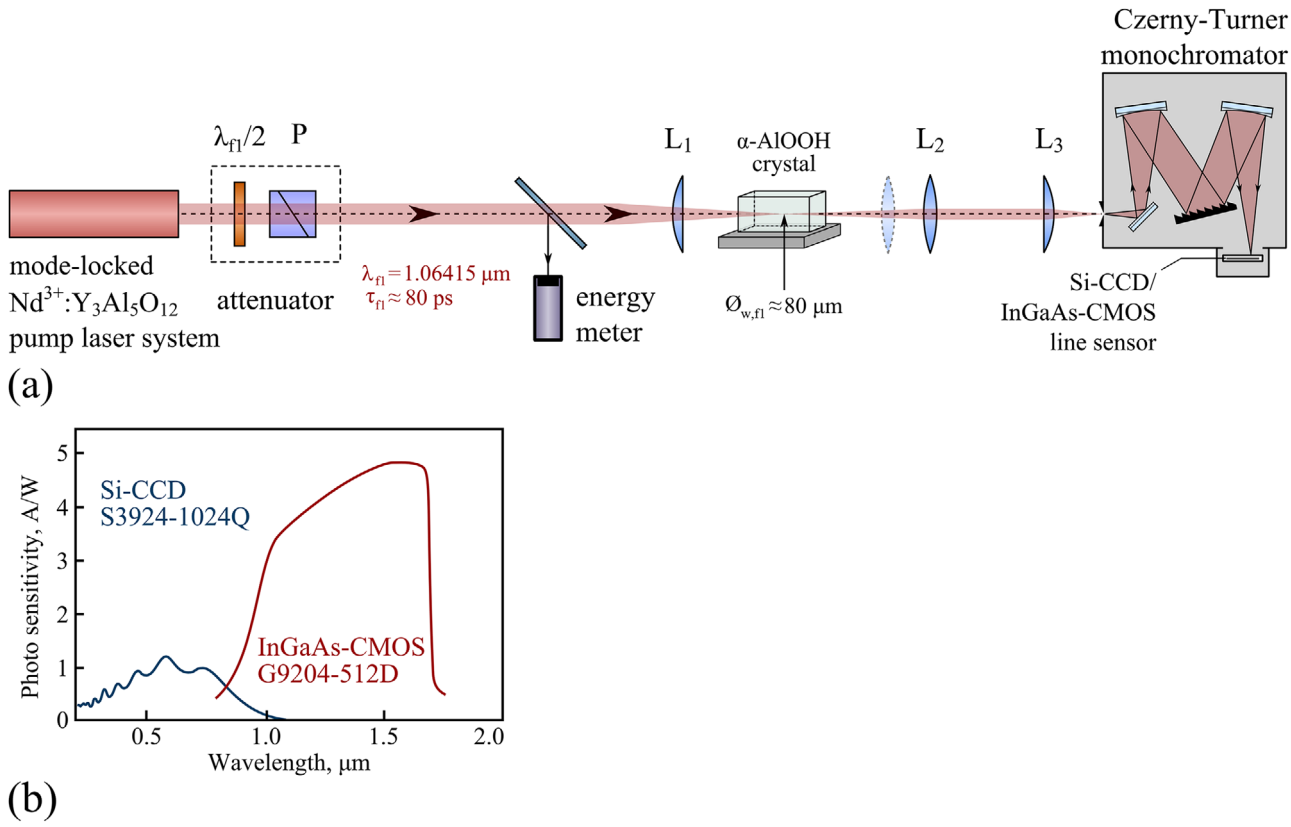

Figure 4. a) Schematic diagram of the experimental setup used for the spectroscopic analysis of SRS and nonlinear mixing interactions in α-AlOOH single crystals (P: polarizer; L_1–L_3: lenses; see also text). b) Spectral sensitivity of the used Si- and InGaAs line sensors (data taken from Hamamatsu Photonics K.K. datasheet).

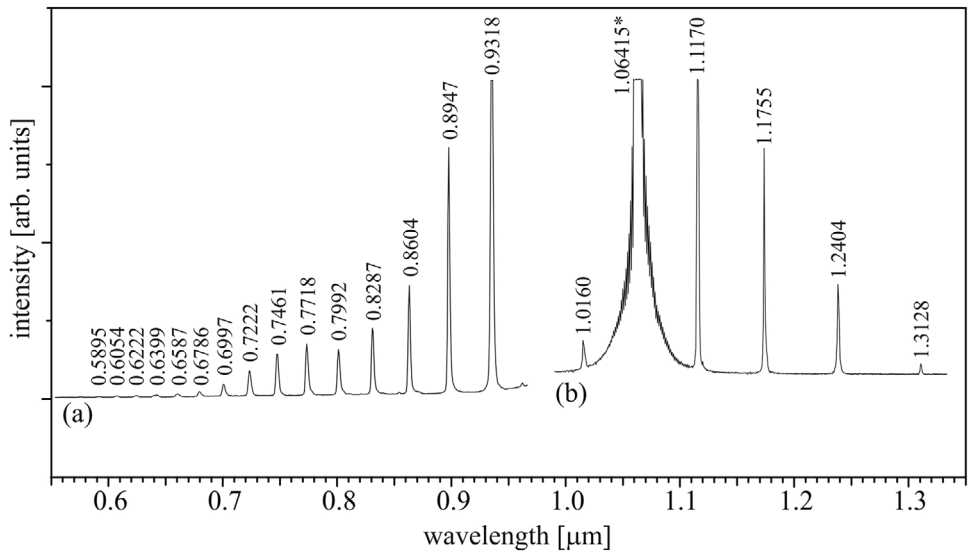

Figure 5. Selected parts of SRS and RFWM lasing spectra of a single crystal of α-AlOOH, recorded at room temperature in excitation geometry $c(a,a)c$ with single-wavelength picosecond pumping at λ_{fl} = 1.06415 μm. The wavelength of all lines (pump line is asterisked) is given in μm, their intensity is shown without correction for the spectral sensitivity of the used recording spectrometric system. Part (a) is recorded with a silicon-CCD sensor, part (b) with an InGaAs sensor. All generated Stokes and anti-Stokes components are related to the SRS-active vibration mode with $\omega_{SRS} \approx 445$ cm^{-1}.

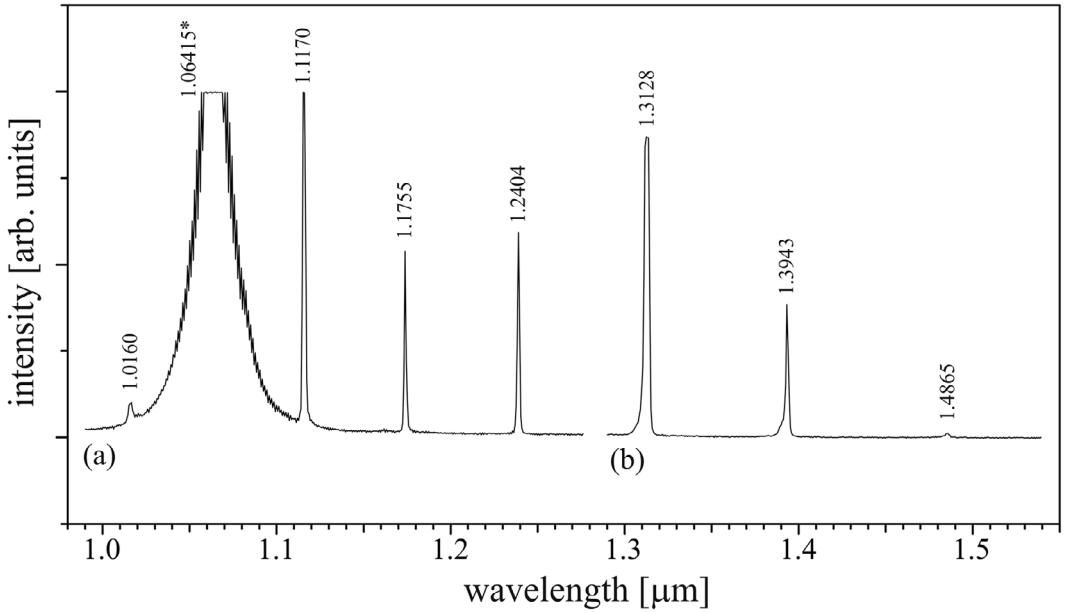

Figure 6. Infrared Stokes generation in an α-AlOOH single crystal under picosecond pumping at λ_{fl} = 1.06415 μm wavelength (pumping wavelength marked with asterisk), using excitation geometry $c(b,b)c$. Wavelengths of all generated Stokes (and anti-Stokes) components are given in μm. Part (a) and (b) are recorded with an InGaAs sensor. All generated components are related to the SRS-active vibration mode with $\omega_{SRS} \approx 445$ cm^{-1}.

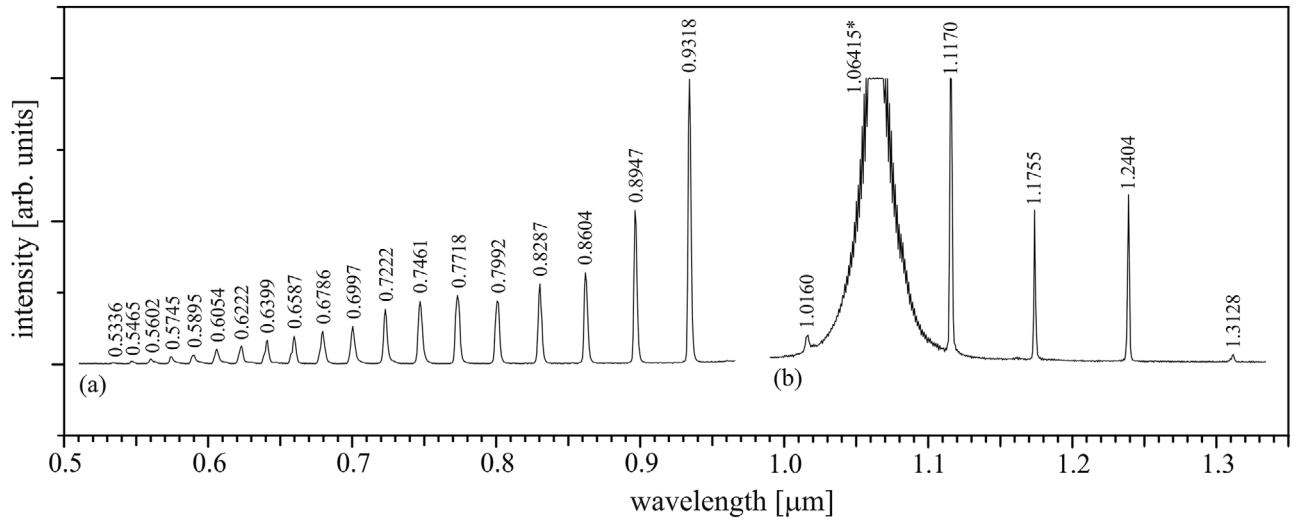

Figure 7. Selected parts of SRS and RFWM lasing spectra of a single crystal of α-AlOOH, recorded at room temperature in excitation geometry $c(b,b)c$ with single-wavelength picosecond pumping at λ_{fl} = 1.06415 μm. The wavelength of all lines (pump line is asterisked) is given in μm, their intensity is shown without correction for the spectral sensitivity of the used recording spectrometric system. Part (a) is recorded with a silicon-CCD sensor and part (b) is recorded with an InGaAs-CCD sensor. All generated Stokes and anti-Stokes components are related to the SRS-active vibration mode with $\omega_{SRS} \approx$ 445 cm^{-1}.

phase-matching conditions lead to a coaxial ring pattern on a screen perpendicular to the propagation direction with the color changing from inside to outside from red via orange, yellow, and green to blue ("anti-Stokes rainbow").

Within the framework of our SRS experiments, we compared the SRS threshold for the first Stokes generation at λ_{St1} = 1.1170 μm in α-AlOOH with that of $GdVO_4$ at λ_{St1-1} = 1.1744 μm, in order to determine the steady-state Raman gain coefficient g_{ssR}^{St1} for the title crystal under pumping at λ_{fl} = 1.06415 μm. This procedure is based on the relation[38,39] $g_{ssR}^{St1} I_p^{th} l_{SRS} \approx 30$, with l and I_p^{th} denoting the sample length and threshold pump intensity that has to be applied for a reliable detection of the first-Stokes signal, respectively. In our experiments we used an α-AlOOH sample of ≈11 mm length in excitation geometry $c(b,b)c$ and a crystal of $GdVO_4$ of similar length (l = 8 mm) as a reference. The g_{ssR}^{St1-1} value of the latter accounts for ≥4.5 cm GW^{-1}.[40] Comparative measurements yielded an about ninefold higher threshold for first Stokes

Table 2. Room-temperature spectral composition of Stokes and anti-Stokes generation components in an α-AlOOH single crystal recorded under picosecond Nd^{3+}:$Y_3Al_5O_{12}$ laser excitation at the fundamental wavelength $\lambda_{f1} = 1.06415$ µm.

Excitation geometry $c(a,a)c$ [a]	SRS and RFWM lasing			
	Wavelength [b] [µm]	Lasing component	Line attribution	SRS and RFWM attribution [c]
Figure 5a	0.5895	ASt_{17}	$\omega_{f1} + 17\omega_{SRS}$	$\omega_{f1} + 17\omega_{SRS} = [\omega_{f1} + (\omega_{f1} + 16\omega_{SRS}) - (\omega_{f1} - \omega_{SRS})] = [\omega_{f1} + \omega_{ASt16} - \omega_{St1}] = \omega_{ASt17}$
	0.6054	ASt_{16}	$\omega_{f1} + 16\omega_{SRS}$	$\omega_{f1} + 16\omega_{SRS} = [\omega_{f1} + (\omega_{f1} + 15\omega_{SRS}) - (\omega_{f1} - \omega_{SRS})] = [\omega_{f1} + \omega_{ASt15} - \omega_{St1}] = \omega_{ASt16}$
	0.6222	ASt_{15}	$\omega_{f1} + 15\omega_{SRS}$	$\omega_{f1} + 15\omega_{SRS} = [\omega_{f1} + (\omega_{f1} + 14\omega_{SRS}) - (\omega_{f1} - \omega_{SRS})] = [\omega_{f1} + \omega_{ASt14} - \omega_{St1}] = \omega_{ASt15}$
	0.6399	ASt_{14}	$\omega_{f1} + 14\omega_{SRS}$	$\omega_{f1} + 14\omega_{SRS} = [\omega_{f1} + (\omega_{f1} + 13\omega_{SRS}) - (\omega_{f1} - \omega_{SRS})] = [\omega_{f1} + \omega_{ASt13} - \omega_{St1}] = \omega_{ASt14}$
	0.6587	ASt_{13}	$\omega_{f1} + 13\omega_{SRS}$	$\omega_{f1} + 13\omega_{SRS} = [\omega_{f1} + (\omega_{f1} + 12\omega_{SRS}) - (\omega_{f1} - \omega_{SRS})] = [\omega_{f1} + \omega_{ASt12} - \omega_{St1}] = \omega_{ASt13}$
	0.6786	ASt_{12}	$\omega_{f1} + 12\omega_{SRS}$	$\omega_{f1} + 12\omega_{SRS} = [\omega_{f1} + (\omega_{f1} + 11\omega_{SRS}) - (\omega_{f1} - \omega_{SRS})] = [\omega_{f1} + \omega_{ASt11} - \omega_{St1}] = \omega_{ASt12}$
	0.6997	ASt_{11}	$\omega_{f1} + 11\omega_{SRS}$	$\omega_{f1} + 11\omega_{SRS} = [\omega_{f1} + (\omega_{f1} + 10\omega_{SRS}) - (\omega_{f1} - \omega_{SRS})] = [\omega_{f1} + \omega_{ASt10} - \omega_{St1}] = \omega_{ASt11}$
	0.7222	ASt_{10}	$\omega_{f1} + 10\omega_{SRS}$	$\omega_{f1} + 10\omega_{SRS} = [\omega_{f1} + (\omega_{f1} + 9\omega_{SRS}) - (\omega_{f1} - \omega_{SRS})] = [\omega_{f1} + \omega_{ASt9} - \omega_{St1}] = \omega_{ASt10}$
	0.7461	ASt_9	$\omega_{f1} + 9\omega_{SRS}$	$\omega_{f1} + 9\omega_{SRS} = [\omega_{f1} + (\omega_{f1} + 8\omega_{SRS}) - (\omega_{f1} - \omega_{SRS})] = [\omega_{f1} + \omega_{ASt8} - \omega_{St1}] = \omega_{ASt9}$
	0.7718	ASt_8	$\omega_{f1} + 8\omega_{SRS}$	$\omega_{f1} + 8\omega_{SRS} = [\omega_{f1} + (\omega_{f1} + 7\omega_{SRS}) - (\omega_{f1} - \omega_{SRS})] = [\omega_{f1} + \omega_{ASt7} - \omega_{St1}] = \omega_{ASt8}$
	0.7992	ASt_7	$\omega_{f1} + 7\omega_{SRS}$	$\omega_{f1} + 7\omega_{SRS} = [\omega_{f1} + (\omega_{f1} + 6\omega_{SRS}) - (\omega_{f1} - \omega_{SRS})] = [\omega_{f1} + \omega_{ASt6} - \omega_{St1}] = \omega_{ASt7}$
	0.8287	ASt_6	$\omega_{f1} + 6\omega_{SRS}$	$\omega_{f1} + 6\omega_{SRS} = [\omega_{f1} + (\omega_{f1} + 5\omega_{SRS}) - (\omega_{f1} - \omega_{SRS})] = [\omega_{f1} + \omega_{ASt5} - \omega_{St1}] = \omega_{ASt6}$
	0.8604	ASt_5	$\omega_{f1} + 5\omega_{SRS}$	$\omega_{f1} + 5\omega_{SRS} = [\omega_{f1} + (\omega_{f1} + 4\omega_{SRS}) - (\omega_{f1} - \omega_{SRS})] = [\omega_{f1} + \omega_{ASt4} - \omega_{St1}] = \omega_{ASt5}$
	0.8947	ASt_4	$\omega_{f1} + 4\omega_{SRS}$	$\omega_{f1} + 4\omega_{SRS} = [\omega_{f1} + (\omega_{f1} + 3\omega_{SRS}) - (\omega_{f1} - \omega_{SRS})] = [\omega_{f1} + \omega_{ASt3} - \omega_{St1}] = \omega_{ASt4}$
	0.9318	ASt_3	$\omega_{f1} + 3\omega_{SRS}$	$\omega_{f1} + 3\omega_{SRS} = [\omega_{f1} + (\omega_{f1} + 2\omega_{SRS}) - (\omega_{f1} - \omega_{SRS})] = [\omega_{f1} + \omega_{ASt2} - \omega_{St1}] = \omega_{ASt3}$ [d]
Figure 5b	1.0160	ASt_1	$\omega_{f1} + \omega_{SRS}$	$\omega_{f1} + \omega_{SRS} = [\omega_{f1} + \omega_{f1} - (\omega_{f1} - \omega_{SRS})] = [\omega_{f1} + \omega_{f1} - \omega_{St1}] = \omega_{ASt1}$
	1.06415	λ_{f1}	ω_{f1}	ω_{f1}
	1.1170	St_1	$\omega_{f1} - \omega_{SRS}$	$\omega_{f1} - \omega_{SRS} = \omega_{St1}$
	1.1755	St_2	$\omega_{f1} - 2\omega_{SRS}$	$\omega_{f1} - 2\omega_{SRS} = [(\omega_{f1} - \omega_{SRS}) - \omega_{SRS}] = \omega_{St2}$
	1.2404	St_3	$\omega_{f1} - 3\omega_{SRS}$	$\omega_{f1} - 3\omega_{SRS} = [(\omega_{f1} - 2\omega_{SRS}) - \omega_{SRS}] = \omega_{St3}$
	1.3128	St_4	$\omega_{f1} - 4\omega_{SRS}$	$\omega_{f1} - 4\omega_{SRS} = [(\omega_{f1} - 3\omega_{SRS}) - \omega_{SRS}] = \omega_{St4}$

[a] Notation is used in analogy to that in ref. [37]: Characters to the left and to the right of the parentheses denote the direction of the wave normal of the incident and of the generated light, respectively, characters within the parentheses give the polarization direction of the incident and the generated light, respectively; [b] Measurement accuracy is ±0.0003 µm; [c] Lines related to cascaded $\chi^{(3)}$-lasing transitions, in square brackets possibilities for nonlinear-laser components of the RFWM process are given; [d] Note that the second anti-Stokes component is not given in Figure 5.

generation in the title crystal. Considering the shorter sample length of the reference crystal, we conclude that the lower limit of the steady-state Raman gain coefficient for first Stokes generation in α-AlOOH at $\lambda_{St1} = 1.1170$ µm is not less than 0.36 cm GW^{-1}. Here, it should be noted that the generation of Stokes and anti-Stokes frequency combs was accomplished for pump energies only slightly above the first Stokes threshold. In particular, higher order anti-Stokes emission was already observed if the pump energy was increased above I_p^{th} by only 5%.

3.3. SRS-Promoting Vibration Mode

A spontaneous Raman spectrum with the same crystal of α-AlOOH, that was used for the SRS investigations, was measured in geometry $c(b,b)c$, using a distributed feedback laser at $\lambda_{exc} = 0.785$ µm as excitation source. The spectrum given in **Figure 9** was recorded in backscattering geometry by means of a fiber-coupled Raman spectrometer (Princeton Instruments, model PI 320) in combination with a Si-CCD detector (Princeton Instruments, model LN/CCD-1024-EHRB/1). The energy axis of the Raman shift was calibrated using polystyrene. The estimated error of the determination of the Raman line positions is 3 cm^{-1}.

The primitive unit cell of the crystal structure of α-AlOOH with symmetry $Pbmn - D_{2h}^{16}$ with $Z = 4$ contains 16 atoms, which gives $3NZ = 48$ vibration modes ($k \approx 0$): 8 A_{1g} + 4 A_{1u} + 8 B_{1g} + 4 B_{1u} + 4 B_{2g} + 8 B_{2u} + 4 B_{3g} + 8B_{3u}. Among them, 24 modes are Raman-active (8 A_{1g} + 8 B_{1g} + 4 B_{2g} + 4 B_{3g}) and 17 modes are IR-active (3 B_{1u} + 7 B_{2u} + 7 B_{3u}), three translation modes (1B_{1u} + 1B_{2u} +1B_{3u}) and four "silent" modes (4 A_{1u}), see also ref. [7]. α-AlOOH has been subject to several spontaneous Raman studies including both, experimental investigations and ab initio calculations.[5,7,8,9] The most intense vibration mode of α-AlOOH in these studies, as well as in our spectrum given in Figure 9, is found in the range between 446 and 449 cm^{-1}. As can be seen from Figure 9 in our spontaneous Raman investigation we determined the Raman shift for this mode to 449(3) cm^{-1}. This mode is assigned in literature to an A_{1g} mode, most probably an Al—O—Al bending mode.[5,7] In our SRS investigation this sharp, strong vibration mode turned out to be the SRS-promoting mode.

4. Conclusion

The present study of nonlinear laser generation via SRS and RFWM processes in natural crystals of α-AlOOH (diaspore) shows that α-AlOOH is a promising material for efficient

Table 3. Room-temperature spectral composition of Stokes and anti-Stokes generation components in an α-AlOOH single crystal recorded under picosecond Nd^{3+}:$Y_3Al_5O_{12}$ laser excitation at the fundamental wavelength $\lambda_{fl} = 1.06415$ µm.

Excitation geometry $c(b,b)c$[a]	SRS and RFWM lasing			
	Wavelength[b] [µm]	Lasing component	Line attribution	SRS and RFWM attribution[c]
Figure 6a	1.0160	ASt_1	$\omega_{fl} + \omega_{SRS}$	$\omega_{fl} + \omega_{SRS} = [\omega_{fl} + \omega_{fl} - (\omega_{fl} - \omega_{SRS})] = [\omega_{fl} + \omega_{fl} - \omega_{St1}] = \omega_{ASt1}$
	1.06415	λ_{fl}	ω_{fl}	ω_{fl}
	1.1170	St_1	$\omega_{fl} - \omega_{SRS}$	$\omega_{fl} - \omega_{SRS} = \omega_{St1}$
	1.1755	St_2	$\omega_{fl} - 2\omega_{SRS}$	$\omega_{fl} - 2\omega_{SRS} = [(\omega_{fl} - \omega_{SRS}) - \omega_{SRS}] = \omega_{St2}$
	1.2404	St_3	$\omega_{fl} - 3\omega_{SRS}$	$\omega_{fl} - 3\omega_{SRS} = [(\omega_{fl} - 2\omega_{SRS}) - \omega_{SRS}] = \omega_{St3}$
Figure 6b	1.3128	St_4	$\omega_{fl} - 4\omega_{SRS}$	$\omega_{fl} - 4\omega_{SRS} = [(\omega_{fl} - 3\omega_{SRS}) - \omega_{SRS}] = \omega_{St4}$
	1.3943	St_5	$\omega_{fl} - 5\omega_{SRS}$	$\omega_{fl} - 5\omega_{SRS} = [(\omega_{fl} - 4\omega_{SRS}) - \omega_{SRS}] = \omega_{St5}$
	1.4865	St_6	$\omega_{fl} - 6\omega_{SRS}$	$\omega_{fl} - 6\omega_{SRS} = [(\omega_{fl} - 4\omega_{SRS}) - \omega_{SRS}] = \omega_{St6}$
Figure 7a	0.5336	ASt_{21}	$\omega_{fl} + 21\omega_{SRS}$	$\omega_{fl} + 21\omega_{SRS} = [\omega_{fl} + (\omega_{fl} + 20\omega_{SRS}) - (\omega_{fl} - \omega_{SRS})] = [\omega_{fl} + \omega_{ASt20} - \omega_{St1}] = \omega_{ASt21}$
	0.5465	ASt_{20}	$\omega_{fl} + 20\omega_{SRS}$	$\omega_{fl} + 20\omega_{SRS} = [\omega_{fl} + (\omega_{fl} + 19\omega_{SRS}) - (\omega_{fl} - \omega_{SRS})] = [\omega_{fl} + \omega_{ASt19} - \omega_{St1}] = \omega_{ASt20}$
	0.5602	ASt_{19}	$\omega_{fl} + 19\omega_{SRS}$	$\omega_{fl} + 19\omega_{SRS} = [\omega_{fl} + (\omega_{fl} + 18\omega_{SRS}) - (\omega_{fl} - \omega_{SRS})] = [\omega_{fl} + \omega_{ASt18} - \omega_{St1}] = \omega_{ASt19}$
	0.5745	ASt_{18}	$\omega_{fl} + 18\omega_{SRS}$	$\omega_{fl} + 18\omega_{SRS} = [\omega_{fl} + (\omega_{fl} + 17\omega_{SRS}) - (\omega_{fl} - \omega_{SRS})] = [\omega_{fl} + \omega_{ASt17} - \omega_{St1}] = \omega_{ASt18}$
	0.5895	ASt_{17}	$\omega_{fl} + 17\omega_{SRS}$	$\omega_{fl} + 17\omega_{SRS} = [\omega_{fl} + (\omega_{fl} + 16\omega_{SRS}) - (\omega_{fl} - \omega_{SRS})] = [\omega_{fl} + \omega_{ASt16} - \omega_{St1}] = \omega_{ASt17}$
	0.6054	ASt_{16}	$\omega_{fl} + 16\omega_{SRS}$	$\omega_{fl} + 16\omega_{SRS} = [\omega_{fl} + (\omega_{fl} + 15\omega_{SRS}) - (\omega_{fl} - \omega_{SRS})] = [\omega_{fl} + \omega_{ASt15} - \omega_{St1}] = \omega_{ASt16}$
	0.6222	ASt_{15}	$\omega_{fl} + 15\omega_{SRS}$	$\omega_{fl} + 15\omega_{SRS} = [\omega_{fl} + (\omega_{fl} + 14\omega_{SRS}) - (\omega_{fl} - \omega_{SRS})] = [\omega_{fl} + \omega_{ASt14} - \omega_{St1}] = \omega_{ASt15}$
	0.6399	ASt_{14}	$\omega_{fl} + 14\omega_{SRS}$	$\omega_{fl} + 14\omega_{SRS} = [\omega_{fl} + (\omega_{fl} + 13\omega_{SRS}) - (\omega_{fl} - \omega_{SRS})] = [\omega_{fl} + \omega_{ASt13} - \omega_{St1}] = \omega_{ASt14}$
	0.6587	ASt_{13}	$\omega_{fl} + 13\omega_{SRS}$	$\omega_{fl} + 13\omega_{SRS} = [\omega_{fl} + (\omega_{fl} + 12\omega_{SRS}) - (\omega_{fl} - \omega_{SRS})] = [\omega_{fl} + \omega_{ASt12} - \omega_{St1}] = \omega_{ASt13}$
	0.6786	ASt_{12}	$\omega_{fl} + 12\omega_{SRS}$	$\omega_{fl} + 12\omega_{SRS} = [\omega_{fl} + (\omega_{fl} + 11\omega_{SRS}) - (\omega_{fl} - \omega_{SRS})] = [\omega_{fl} + \omega_{ASt11} - \omega_{St1}] = \omega_{ASt12}$
	0.6997	ASt_{11}	$\omega_{fl} + 11\omega_{SRS}$	$\omega_{fl} + 11\omega_{SRS} = [\omega_{fl} + (\omega_{fl} + 10\omega_{SRS}) - (\omega_{fl} - \omega_{SRS})] = [\omega_{fl} + \omega_{ASt10} - \omega_{St1}] = \omega_{ASt11}$
	0.7222	ASt_{10}	$\omega_{fl} + 10\omega_{SRS}$	$\omega_{fl} + 10\omega_{SRS} = [\omega_{fl} + (\omega_{fl} + 9\omega_{SRS}) - (\omega_{fl} - \omega_{SRS})] = [\omega_{fl} + \omega_{ASt9} - \omega_{St1}] = \omega_{ASt10}$
	0.7461	ASt_9	$\omega_{fl} + 9\omega_{SRS}$	$\omega_{fl} + 9\omega_{SRS} = [\omega_{fl} + (\omega_{fl} + 8\omega_{SRS}) - (\omega_{fl} - \omega_{SRS})] = [\omega_{fl} + \omega_{ASt8} - \omega_{St1}] = \omega_{ASt9}$
	0.7716	ASt_8	$\omega_{fl} + 8\omega_{SRS}$	$\omega_{fl} + 8\omega_{SRS} = [\omega_{fl} + (\omega_{fl} + 7\omega_{SRS}) - (\omega_{fl} - \omega_{SRS})] = [\omega_{fl} + \omega_{ASt7} - \omega_{St1}] = \omega_{ASt8}$
	0.7992	ASt_7	$\omega_{fl} + 7\omega_{SRS}$	$\omega_{fl} + 7\omega_{SRS} = [\omega_{fl} + (\omega_{fl} + 6\omega_{SRS}) - (\omega_{fl} - \omega_{SRS})] = [\omega_{fl} + \omega_{ASt6} - \omega_{St1}] = \omega_{ASt7}$
	0.8287	ASt_6	$\omega_{fl} + 6\omega_{SRS}$	$\omega_{fl} + 6\omega_{SRS} = [\omega_{fl} + (\omega_{fl} + 5\omega_{SRS}) - (\omega_{fl} - \omega_{SRS})] = [\omega_{fl} + \omega_{ASt5} - \omega_{St1}] = \omega_{ASt6}$
	0.8604	ASt_5	$\omega_{fl} + 5\omega_{SRS}$	$\omega_{fl} + 5\omega_{SRS} = [\omega_{fl} + (\omega_{fl} + 4\omega_{SRS}) - (\omega_{fl} - \omega_{SRS})] = [\omega_{fl} + \omega_{ASt4} - \omega_{St1}] = \omega_{ASt5}$
	0.8947	ASt_4	$\omega_{fl} + 4\omega_{SRS}$	$\omega_{fl} + 4\omega_{SRS} = [\omega_{fl} + (\omega_{fl} + 3\omega_{SRS}) - (\omega_{fl} - \omega_{SRS})] = [\omega_{fl} + \omega_{ASt3} - \omega_{St1}] = \omega_{ASt4}$
	0.9318	ASt_3	$\omega_{fl} + 3\omega_{SRS}$	$\omega_{fl} + 3\omega_{SRS} = [\omega_{fl} + (\omega_{fl} + 2\omega_{SRS}) - (\omega_{fl} - \omega_{SRS})] = [\omega_{fl} + \omega_{ASt2} - \omega_{St1}] = \omega_{ASt3}$[d]
Figure 7b	1.0160	ASt_1	$\omega_{fl} + \omega_{SRS}$	$\omega_{fl} + \omega_{SRS} = [\omega_{fl} + \omega_{fl} - (\omega_{fl} - \omega_{SRS})] = [\omega_{fl} + \omega_{fl} - \omega_{St1}] = \omega_{ASt1}$
	1.06415	λ_{fl}	ω_{fl}	ω_{fl}
	1.1170	St_1	$\omega_{fl} - \omega_{SRS}$	$\omega_{fl} - \omega_{SRS} = \omega_{St1}$
	1.1755	St_2	$\omega_{fl} - 2\omega_{SRS}$	$\omega_{fl} - 2\omega_{SRS} = [(\omega_{fl} - \omega_{SRS}) - \omega_{SRS}] = \omega_{St2}$
	1.2404	St_3	$\omega_{fl} - 3\omega_{SRS}$	$\omega_{fl} - 3\omega_{SRS} = [(\omega_{fl} - 2\omega_{SRS}) - \omega_{SRS}] = \omega_{St3}$
	1.3128	St_4	$\omega_{fl} - 4\omega_{SRS}$	$\omega_{fl} - 4\omega_{SRS} = [(\omega_{fl} - 3\omega_{SRS}) - \omega_{SRS}] = \omega_{St4}$

[a] Notation is used as in Table 2; [b] Measurement accuracy is ±0.0003 µm; [c] Lines related to cascaded $\chi^{(3)}$-lasing transitions, in square brackets possibilities for nonlinear-laser components of the RFWM process are given; [d] Note that the second anti-Stokes component is not given in Figure 7.

broadband lasing comb generation. Similar as for α-Al_2O_3 (corundum) in crystals of α-AlOOH the $\chi^{(3)}$-nonlinear lasing arises from a single SRS-promoting vibration mode, here, with an energy of $\omega_{SRS} \approx 445$ cm^{-1}, which corresponds to the dominant fully symmetric A_{1g} mode observed in spontaneous Raman spectra of diaspore. The investigations give no hints to SRS-activity of O—H stretching modes in the intermediate hydrogen bonds present in the crystal structure of α-AlOOH. The results of the SRS study reveal that α-AlOOH can be classified as an attractive material for effective $\chi^{(3)}$-nonlinear lasing, which provides lasing wavelengths that are not available from nonlinear optical processes so far. Since at present only natural single crystals of diaspore of optical quality and sufficient dimensions are accessible, these promising results may encourage efforts to grow large single crystals of α-AlOOH by hydrothermal methods in the future.

Acknowledgements

Open access funding enabled and organized by Projekt DEAL.

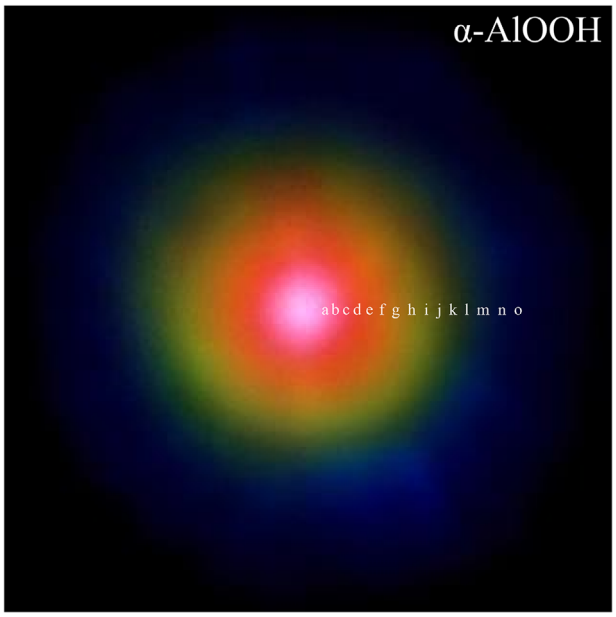

Figure 8. Conical multiwavelength emission resulting from anti-Stokes RFWM processes in an α-AlOOH single crystal ("anti-Stokes rainbow"). The picture was taken at room temperature in excitation geometry $c(b,b)c$ under picosecond pumping at $\lambda_{f1} = 1.06415$ µm wavelength using a CCD photocamera (Panasonic Lumix DMC-TZ7). The numbers indicate the respective anti-Stokes components related to the SRS-promoting vibrational mode $\omega_{SRS} \approx 445$ cm^{-1} as follows: a: $\lambda_{ASt11} = 0.6997$ µm, b: $\lambda_{ASt12} = 0.6786$ µm, c: $\lambda_{ASt13} = 0.6587$ µm, d: $\lambda_{ASt14} = 0.6399$ µm, e: $\lambda_{ASt15} = 0.6222$ µm, f: $\lambda_{ASt16} = 0.6054$ µm, g: $\lambda_{ASt17} = 0.5895$ µm, h: $\lambda_{ASt18} = 0.5745$ µm, i: $\lambda_{ASt19} = 0.5602$ µm, j: $\lambda_{ASt20} = 0.5465$ µm, k: $\lambda_{ASt21} = 0.5336$ µm, l: $\lambda_{ASt22} = 0.5212$ µm, m: $\lambda_{ASt23} = 0.5094$ µm, n: $\lambda_{ASt24} = 0.4981$ µm, and o: $\lambda_{ASt25} = 0.4873$ µm. See also the corresponding spectrum in Figure 7.

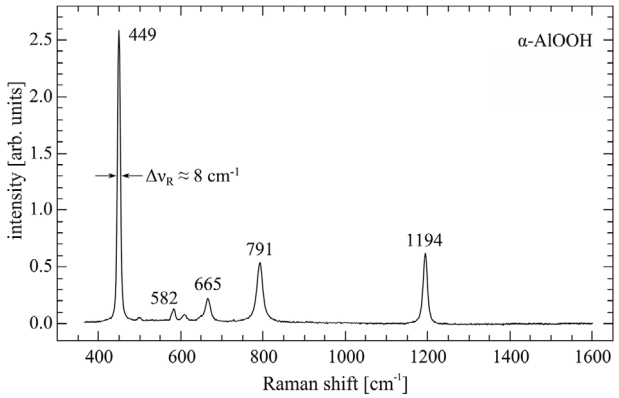

Figure 9. Polarized spontaneous Raman scattering spectrum of an α-AlOOH single crystal. The spectrum was recorded at room temperature under excitation at 0.785 µm wavelength in geometry $c(b,b)c$ using a Princeton Instruments spectrometer (model PI 320) in combination with a Si-CCD detector (Princeton Instruments, model LN/CCD-1024-EHRB/1). The energy of selected Raman shifted lines is given in cm^{-1}. The determined linewidth $\Delta\nu_R$ (FWHM) of the SRS-promoting vibrational mode at ≈449 cm^{-1} is limited by the instrument resolution.

Conflict of Interest

The authors declare no conflict of interest.

Data Availability Statement

Research data are not shared.

Keywords

α-AlOOH, broadband lasing comb generation, diaspore, stimulated Raman scattering

Received: March 29, 2021
Revised: July 7, 2021
Published online: September 16, 2021

[1] A. A. Kaminskii, *Laser Photonics Rev.* **2007**, *1*, 93.
[2] A. A. Kaminskii, L. Bohatý, P. Becker, H. J. Eichler, H. Rhee, *Phys.-Usp.* **2008**, *51*, 899.
[3] A. A. Kaminskii, H. J. Eichler, D. Grebe, R. Macdonald, A. V. Butashin, *Phys. Status Solidi B* **1997**, *199*, R3.
[4] A. A. Kaminskii, A. V. Butashin, S. N. Bagaev, H. J. Eichler, D. Grebe, R. Macdonald, *Quantum Electron.* **1997**, *27*, 612.
[5] H. D. Ruan, R. L. Frost, J. T. Kloprogge, *J. Raman Spectrosc.* **2001**, *32*, 745.
[6] B. Winkler, A. Friedrich, D. J. Wilson, E. Haussühl, M. Krisch, A. Bosak, K. Refson, V. Milman, *Phys. Rev. Lett.* **2008**, *101*, 065501.
[7] R. Demichelis, Y. Noel, B. Civalleri, C. Roetti, M. Ferrero, R. Dovesi, *J. Phys. Chem. B* **2007**, *111*, 9337.
[8] R. E. San Juan-Farfán, L. Bayarjargal, B. Winkler, E. Haussühl, M. Avalos-Borja, K. Refson, V. Milman, *Phys. Chem. Miner.* **2011**, *38*, 693.
[9] S. Delattre, E. Balan, M. Lazzeri, M. Blanchard, M. Guillaumet, O. Beyssac, E. Haussühl, B. Winkler, E. K. H. Salje, G. Calas, *Phys. Chem. Miner.* **2012**, *39*, 93.
[10] A. Z. Grasyuk, S. V. Kurbasov, L. L. Losev, A. P. Lutsenko, A. A. Kaminskii, V. B. Semenov, *Quantum Electron.* **1998**, *28*, 162.
[11] A. A. Kaminskii, L. Bohatý, P. Becker, P. Held, H. Rhee, H. J. Eichler, J. Hanuza, *Laser Phys. Lett.* **2009**, *6*, 335.
[12] W. F. de Jong, *Natuurwet. Tijdschr.* **1930**, *12*, 69.
[13] M. Deflandre, *Bull. Soc. Franç. Minér.* **1932**, *55*, 140.
[14] K. Takané, *Proc. Imp. Acad. Tokyo* **1933**, *9*, 113.
[15] F. J. Ewing, *J. Chem. Phys.* **1935**, *3*, 203.
[16] W. Hoppe, *Z. Kristallogr.* **1940**, *103*, 73.
[17] W. Hoppe, *Z. Kristallogr.* **1942**, *104*, 11.
[18] W. R. Busing, H. A. Levy, *Acta Crystallogr.* **1958**, *11*, 798.
[19] *Inorganic Crystal Structure Database ICSD*, Leibniz-Institut für Informationsinfrastruktur GmbH, FIZ-Karlsruhe, **2021**.
[20] R. J. Hill, *Phys. Chem. Miner.* **1979**, *5*, 179.
[21] A. W. Laubengayer, R. S. Weisz, *J. Am. Chem. Soc.* **1943**, *65*, 247.
[22] G. C. Kennedy, *Am. J. Sci.* **1950**, *257*, 563.
[23] K. Torkar, H. Krischner, *Monatsh. Chem.* **1960**, *91*, 764.
[24] S. Matsushima, G. C. Kennedy, J. Akella, J. Haygarth, *Am. J. Sci.* **1967**, *265*, 28.
[25] J. F. W. Bowles, R. A. Howie, D. J. Vaughan, J. Zussman, *Rock-Forming Minerals, Non-Silicates: Oxides, Hydroxides and Sulphides, Vol. 5A*, The Geological Society, London **2011**, pp. 546–563.
[26] A. R. Pawley, S. A. T. Redfern, T. J. B. Holland, *Am. Mineral.* **1996**, *81*, 335.
[27] W. Wilson, T. P. Moore, *Mineral. Rec.* **2020**, *51*, 541.
[28] C. Shen, R. Lu, *Gems Gemol.* **2018**, *54*, 394 .

[29] R. D. Shannon, R. C. Shannon, O. Medenbach, R. X. Fischer, *J. Phys. Chem. Ref. Data* **2002**, *31*, 931.
[30] J. J. Krebs, W. G. Maisch, *Phys. Rev. B* **1971**, *4*, 757.
[31] J. Ferguson, P. E. Fielding, *Chem. Phys. Lett.* **1971**, *10*, 262.
[32] O. Medenbach, R. D. Shannon, *J. Opt. Soc. Am. B* **1997**, *14*, 3299.
[33] S. Haussühl, *Z. Kristallogr.* **1993**, *204*, 67.
[34] J. W. Anthony, R. A. Bideaux, K. W. Bladh, M. C. Nichols, *Handbook of Mineralogy*, Mineral Data Publishing, Tucson, AZ **1990**.
[35] A. A. Kaminskii, O. Lux, H. Rhee, H. J. Eichler, K. Ueda, H. Yoneda, A. Shirakawa, B. Zhao, J. Chen, J. Dong, J. Zhang, *Laser Phys. Lett.* **2012**, *9*, 879.
[36] A. A. Kaminskii, O. Lux, H. Rhee, H. J. Eichler, H. Yoneda, A. Shirakawa, K. Ueda, R. Rückamp, L. Bohatý, P. Becker, *Laser Phys. Lett.* **2013**, *10*, 073001.
[37] T. C. Damen, S. P. S. Porto, B. Tell, *Phys. Rev.* **1966**, *142*, 570.
[38] W. Kaiser, M. Maier, in *Laser Handbook*, Vol. *2* (Eds: F. T. Arecchi, E. O. Schulz-Dubois), North-Holland Publishing, Amsterdam **1972**, p. 1077.
[39] Y. R. Shen, *The Principles of Nonlinear Optics*, Wiley, New York **1984**.
[40] A. A. Kaminskii, K. Ueda, H. J. Eichler, Y. Kuwano, H. Kouta, S. N. Bagaev, T. H. Chiba, J. C. Barnes, G. M. A. Gad, T. Murai, J. Lu, *Opt. Commun.* **2001**, *194*, 201.